www.czasopisma.pan.pl PAN www.journals.pan.pl

INTL JOURNAL OF ELECTRONICS AND TELECOMMUNICATIONS, 2019, VOL. 65, NO. 1, PP. 57-64
Manuscript received May 7, 2018; revised January, 2019. DOI: 10.24425/ijet.2019.126283

Active Inductor with Feedback Resistor Based Voltage Controlled Oscillator Design for Wireless Applications

Omar Faruqe, and Md Tawfiq Amin

***Abstract*—This paper presents active inductor based VCO design for wireless applications based on analysis of active inductor models (Weng-Kuo Cascode active inductor & Liang Regular Cascode active inductor) with feedback resistor technique. Embedment of feedback resistor results in the increment of inductance as well as the quality factor whereas the values are 125.6@2.4GHz (Liang) and 98.7@3.4GHz (Weng-Kuo). The Weng-Kuo active inductor based VCO shows a tuning frequency of 1.765GHz ~2.430GHz (31.7%), while consuming a power of 2.60 mW and phase noise of -84.15 dBc/Hz@1MHz offset. On the other hand, Liang active inductor based VCO shows a frequency range of 1.897GHz ~2.522GHz (28.28%), while consuming a power of 1.40 mW and phase noise of -80.79 dBc/Hz@1MHz offset. Comparing Figure-of-Merit (FoM), power consumption, output power and stability in performance, designed active inductor based VCOs outperform with the state-of-the-art.**

***Keywords*—VCO, active inductor, inductance, quality factor, phase noise, figure-of-merit**

I. Introduction

IN the modern wireless communication system, the voltage controlled oscillator (VCO) exhibits a very outstanding contribution and has become counterpart in this sector [1]. VCO is a fundamental comprising element of PLL (Phase Locked Loop), which is the basic building block of RF transceiver [2]. Furthermore, the frequency synthesizers, high efficient transmitter, ADC (analog–to–digital converter), local oscillator have a fundamental inclusive part, VCO [3-6]. Small silicon area, low power consumption, low phase noise and wide tuning range are the basic performance parameters of a VCO. Ring Oscillator and LC oscillator are mostly used for high frequency applications. Small silicon area consumption and wide frequency range are the two key advantages of the ring oscillator. But it has a main drawback of poor phase noise performance, whereas LC VCO has the ability to surmount this drawback.

However, LC VCO exhibits a low tuning scope and has a very high silicon area consumption which emerges due to spiral or passive inductor [7]. This drawback can be overcome by replacing the passive inductor with active inductor. Moreover, in perspective of quality factor, silicon area consumption and tunibity the active inductor outperforms the spiral inductor [8]. The active inductor basically utilizes the Gyrator-C topology, which is in feedback configuration. By embedding a resistor (R_f) in the feedback path a good contribution in the improvement of quality factor can be achieved, thereby in phase noise performance.

Authors are with Military Institute of Science and technology (MIST), Dhaka, Bangladesh (e-mail: ofaruqe20@gmail.com, tawfiqamin@gmail.com).

This writing has a seven consisting section where section II expatiates various active inductor topologies with and without feedback resistor. Section III explicates the simulation and corresponding results, graphs. The designs are proposed at section IV. Section V contains a broad clarification, discussion and comparison of simulation results of the proposed VCOs, which is concluded by section VI.

II. Active Inductor Topologies

A. Basic Gyrator- C Active inductor:

A Gyrator-C active inductor is formed by two consecutive transconductors (for example MOSFET) with one terminal is connected to a capacitor. It can be designated as single ended if one port is connected to a ground or any power supply [9]. The schematic representation (Fig.1) and the corresponding equations are given below.

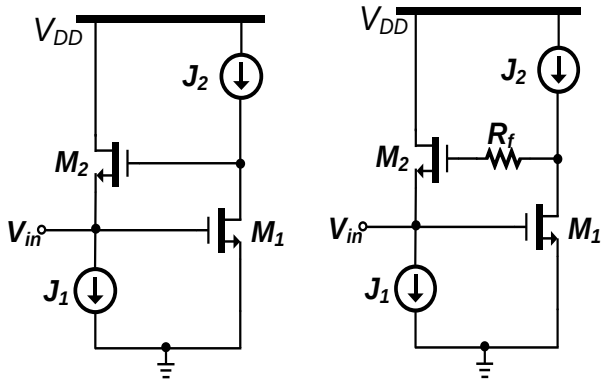

(a) (b)

Fig. 1. Schematic representation of Basic Gyrator- C active inductor. (a) Without feedback resistor. (b) With feedback resistor.

$$Z_{in}=\frac{(g_{ds2}g_{m1})+s(C_{gs2}+C_{gd2}+C_{gd1})}{(sC_{gd2}+g_{ds2}+g_{m2})\,(s(C_{gs2}+C_{gd1})+g_{m2})}$$

$$G=g_{ds2}+g_{m1}\approx g_{m1},\quad L=\frac{C_{gs2}}{g_{m1}g_{m2}} \qquad (1)$$

$$R_s=\frac{g_{ds1}}{g_{m1}g_{m2}},\ C=C_{gs1}$$

The self-resonant frequency is given by, $\omega_o=\sqrt{\frac{g_{m1}g_{m2}}{C_{gs1}C_{gs2}}}$

The equations stated above are the expressions for equivalent input impedance, conductance, inductance, series resistance, parallel capacitance and self-resonant frequency. As the Q factor is the ratio of the imaginary part and real part of

impedance, then by improving the inductance without affecting others a high-Q factor active inductor can be accomplished. Therefore, a new technique, that is employment of a feedback resistor from the drain output of M_1 to the gate input of M_2, shows a tremendous contribution in this case. [9]

$$G \approx g_{ds2} + \frac{g_{m1}}{1+R_f g_{ds1}}$$

$$L \approx \frac{C_{gs2}(1+R_f g_{ds1})}{g_{m1} g_{m2}},\ R_s \approx \frac{g_{ds1}}{g_{m1} g_{m2}} \text{ and } C \approx C_{gs1} \qquad (2)$$

Now the new analyzed resonant frequency can be expressed by the equation given below

$$\omega_o = \sqrt{\frac{g_{m1} g_{m2}}{C_{gs1} C_{gs2}(1+R_f g_{ds1})}}$$

Equations (2) are the corresponding equations of G,L, R_s and C. It is clear that the inductance is increased by a factor of $(1 + R_f g_{ds1})$ which results in the increment of the quality factor. Moreover, another major contributing factor of quality factor R_s remains constant and so it has no impact on the quality factor. [9]

B. Weng-Kuo Cascode Active Inductor:

An active inductor which utilizes the current reuse cascode was introduced by Weng and Kuo. The noteworthy advantage of this topology is that, it provides the scope of tuning inductance and quality factor independently [10]. The schematic representation of Weng-Kuo Cascode Active Inductor is depicted in Fig. 2

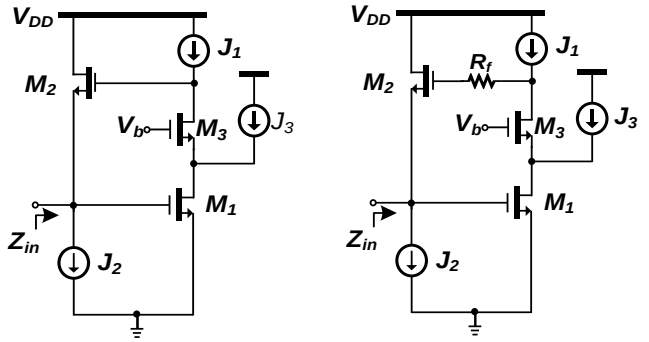

Fig. 2. Weng- Kuo Cascode active inductor. (a) Without feedback resistor. (b) With feedback resistor.

Here g_{m1} is relative to $J_1 + J_3$ but g_{m3} just corresponding to J_1 . The other equations are cited below

$$L = \frac{C_{gs2}}{g_{m1} g_{m2}}, R_s = \frac{g_{ds1} g_{ds3}}{g_{m1} g_{m2} g_{m3}}$$

$$C = C_{gs1},\ G = g_{ds2} + g_{m1} \approx g_{m1} \qquad (3)$$

The resonant frequency and the quality factor at resonant frequency are given by

$$\omega_o = \sqrt{\frac{g_{m1} g_{m2}}{C_{gs1} C_{gs2}}}$$

and $$Q(\omega_o) = \frac{\omega_0 L}{R_s} = \frac{g_{m3}}{g_{ds1} g_{ds3}} \sqrt{\frac{g_{m1} g_{m2} C_{gs2}}{C_{gs1}}}$$

Tunibilty of ω_o can be achieved by variation of g_{m1} and g_{m2}, but for Q variation of g_{m3} is enough. So the tunibility of Q will no longer depends on ω_o [10].

Now introduction of a feedback resistor as in the previous case will generate a quite different condition. The analyzed equations for employing the feedback resistor from the drain output of M_3 to the gate input of M_2 are given below.

$$L \approx \frac{C_{gs2}(1+R_f g_{ds1})}{g_{m1} g_{m2}},\ R_s \approx \frac{g_{ds1} g_{ds3}}{g_{m1} g_{m2} g_{m3}}$$

$$C \approx C_{gs1},\ G \approx g_{ds2} + \frac{g_{m1}}{1+R_f g_{ds1}} \qquad (4)$$

$$\omega_o = \sqrt{\frac{g_{m1} g_{m2}}{C_{gs1} C_{gs2}(1+R_f g_{ds1})}}$$

and $$Q(\omega_o) = \frac{\omega_0 L}{R_s} = \frac{g_{m3}}{g_{ds1} g_{ds3}} \sqrt{\frac{g_{m1} g_{m2} C_{gs2}(1+R_f g_{ds1})}{C_{gs1}}}$$

C. Liang Feedback resistance regular cascode active inductor:

The performance of Weng-Kuo active inductor can be further improved by replacing the cascode with a regular cascode. The idea of using regulated cascade was introduced in Manetakis Regulated Cascode Active Inductor [11]. Again it was further upgraded by J. Liang, where a feedback resistor was embedded [12]. The analysis of both cases will show the effect of regulated cascode and regulated cascode with feedback resistor.

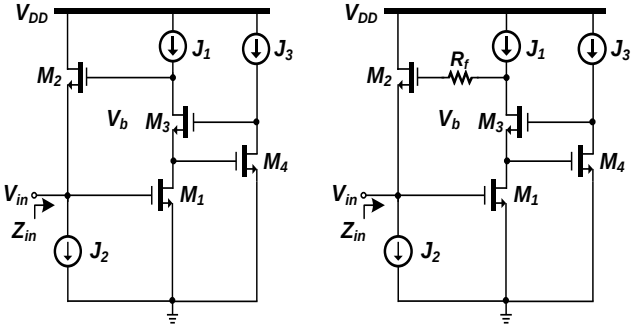

Fig. 3 . (a) Manetakis regular cascode active inductor. (b) Liang feedback resistor regular cascode active inductor.

Manetakis regulated cascode active inductor employs two MOSs M_3 and M_4 which will ultimately reduce the series resistance R_s cause the increment of the Q factor [11]. The corresponding equations are given below

$$L = \frac{C_{gs2}}{g_{m1} g_{m2}}, R_s = \frac{g_{ds3} g_{ds4}}{g_{ds1} g_{m1} g_{m2} g_{m3} g_{m4}}$$

$$C = C_{gs1}, G = g_{ds2} + g_{m1} \approx g_{m1} \qquad (5)$$

The resonant frequency and the quality factor at resonant frequency are given by

$$\omega_o = \sqrt{\frac{g_{m1}g_{m2}}{C_{gs1}C_{gs2}}}$$

and $$Q(\omega_o) = \frac{\omega_0 L}{R_s} = \frac{g_{ds1}g_{m3}g_{m4}}{g_{ds3}g_{ds4}} \sqrt{\frac{g_{m1}g_{m2}C_{gs2}}{C_{gs1}}}$$

The employment feedback resistor R_s will cause further improvement in the Q factor due to increment of the inductance [12]. The corresponding equations are given below.

$$L \approx \frac{C_{gs2}(1+R_f g_{ds1})}{g_{m1}g_{m2}}, R_s \approx \frac{g_{ds3}g_{ds4}}{g_{ds1}g_{m1}g_{m2}g_{m3}g_{m4}}$$

$$C \approx C_{gs1} \ , \ G \approx g_{ds2} + \frac{g_{m1}}{1+R_f g_{ds1}} \qquad (6)$$

$$\omega_o = \sqrt{\frac{g_{m1}g_{m2}}{C_{gs1}C_{gs2}(1+R_f g_{ds1})}}$$

and $$Q(\omega_o) = \frac{\omega_0 L}{R_s}$$

$$= \frac{g_{ds1}g_{m3}g_{m4}}{g_{ds3}g_{ds4}} \sqrt{\frac{g_{m1}g_{m2}C_{gs2}(1+R_f g_{ds1})}{C_{gs1}}}$$

III. Simulation of Active Inductor

Since the ideal current sources J_1, J_2 and J_3 are impractical, so these will be replaced by saturated MOSs, which act as current source. The s parameter simulation was performed to achieve the graph of inductance and Q factor.The value of feedback resistor is 1KΩ. The new schematic diagram of Weng-Kuo Cascode Active Inductor and Liang Feedback resistance regular cascade active inductor with saturated MOS as current source along with W/L ratios are shown in Fig. 4.

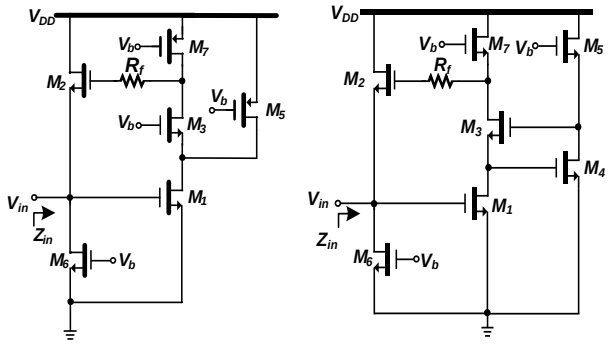

Fig. 4. (a) Weng Kuo cascode active inductor with saturated MOS as current sources. (b) Liang feedback resistor regular cascode active inductor with saturated MOSs as current sources.

The simulation is performed with a power supply of V_{DD}=1V and a biasing voltage of V_b=0.5 V. For all saturated pMOSs as current sources the $\frac{W}{L} = 4\mu m/120nm$ and nMOSs $\frac{W}{L} = 6\mu m/300nm$ are used.

TABLE I
Widths and Lengths of Implemented Transistors

MOS	Width(μm)	Length(nm)
M_1	12	120
M_2	22	140
M_3	25	140
M_5	4	120
M_6	6	300
M_7	4	120
M_4	4.2	300

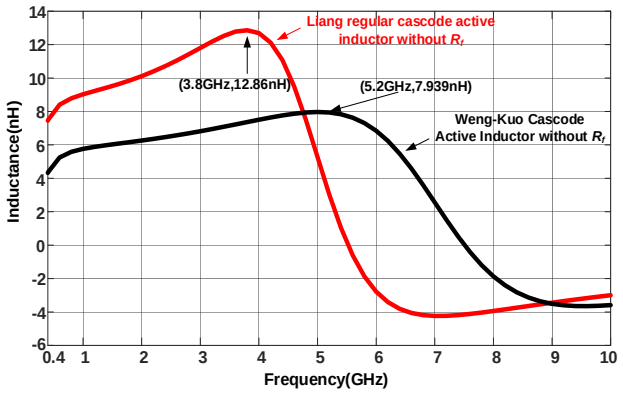

Fig. 5 (a). Graphical representation of inductance vs frequency of selected active inductors.

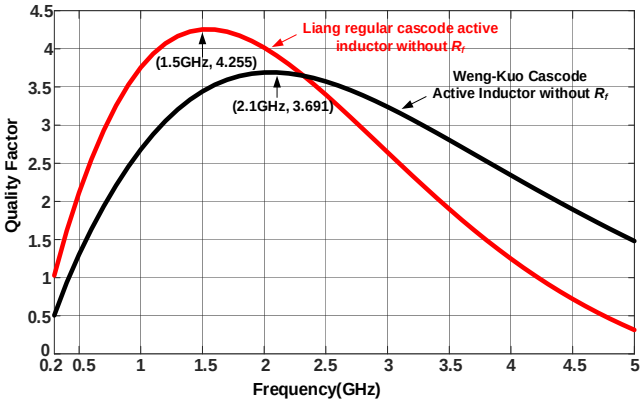

Fig. 5 (b). Graphical representation of quality factor vs frequency of selected active inductors.

From fig. 5(b), it can be seen that the quality factor of Liang regular cascode active inductor is greater than the Weng-Kuo active inductor. It occurs as the inductive value is greater in case of first one than the second. Again the series resistance R_s is divided an additional terms g_{ds1}, $g_{m3}$and g_{m4} due to regular cascode in Liang regular cascode active inductor. These two effects have an overall contribution in the increment of Q factor for Liang regular cascode active inductor. The maximum inductive values are 12.86nH@3.8 GHz (Liang) and 7.94nH @5.2GHz (Weng-Kuo). Similarly, the maximum Q factors are 4.26@1.5 GHz (Liang) and 3.69@2.1GHz.

Figure 6 depicts the case where the resistor is imbedded. As the inductance is increased by a factor of $(1 + R_f g_{ds1})$, so the numerical values of maximum inductance increase to 30.9nH and 27nH in both cases. Now the upgraded values of quality factors are 125.6@2.4GHz (Liang) and 98.7@3.4GHz (Weng-Kuo). The power consumption is 429.9μW for Liang regular cascode, where it is 474.1 μW fow Weng Kuo cascode active inductor.

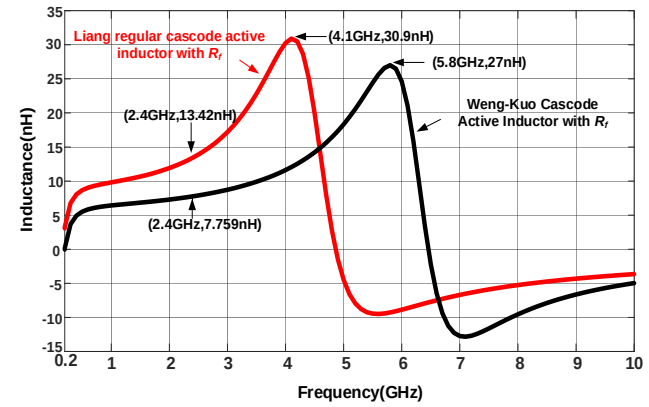

Fig. 6 (a). Graphical representation of quality factor vs frequency of selected active inductors with feedback resistor

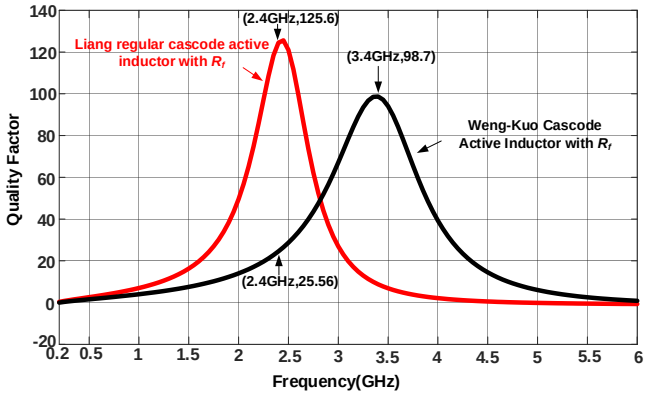

Fig. 6 (b). Graphical representation of quality factor vs frequency of selected active inductors with feedback resistor.

IV. NMOS LC VCO Topology and Proposed Active Inductor Based VCOs

LC VCO topology is formed by inductors in differential configuration, cross-coupled NMOS transistor's pair, a varactor and a current source as shown in Fig. 7. Every section of this formation has its particular contribution. The inductor's own parasitic capacitance and the varactor form the LC tank where the varactor is used to vary the oscillation frequency. In practical case, the LC tank has its own resistance which is responsible for the diminishing of the oscillation. Therefore, a high gain amplification, which is the fundamental requirement for sustaining the oscillation.

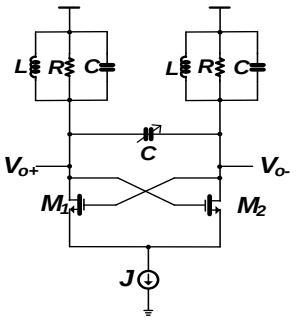

Fig. 7: Simplified Schematic of NMOS cross coupled LC VCO topology.

The cross-coupled NMOSs (M_1 *and* M_2), which are back to back connected in common source configuration provide the large voltage gain. This configuration has another major duty that it provides a phase shift of -360 degree that is one of the basic postulates of Barkhausen Criteria. Therefore two basic conditions first one is a large voltage gain and the second one is total phase shift of -360 are fulfilled by this cross coupled configuration. The residuum, that is the tail current source J is used to regulate the resistance of the MOSs, so that the desired voltage gain can be accomplished for sustaining the oscillation [13]. This topology will be used for the subsequent design purpose.

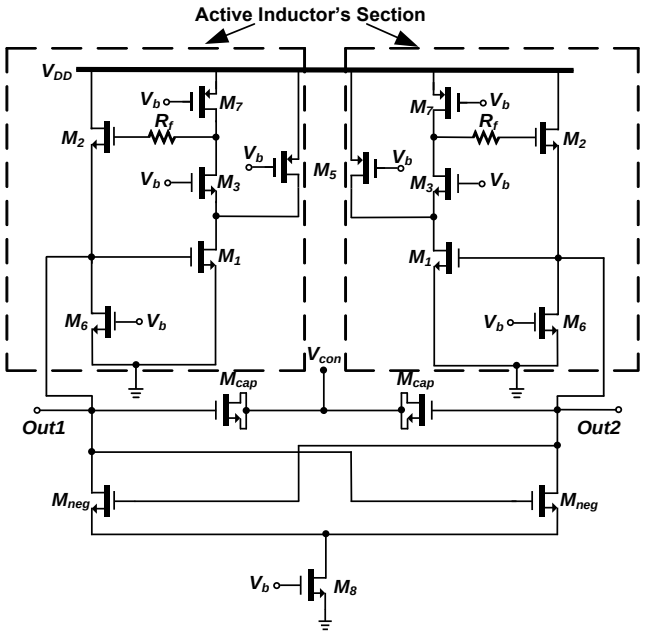

Fig. 8(a) Schematic diagram of Weng-Kuo cascode active inductor based VCO employing feedback resistor topology.

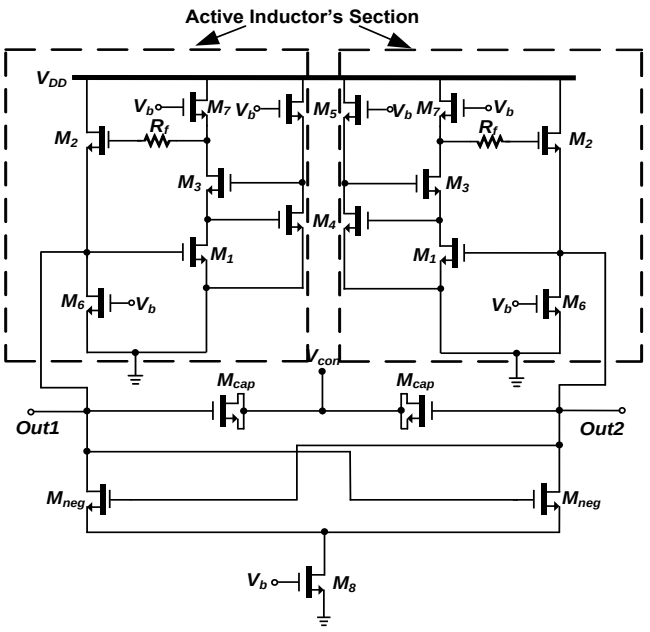

Figure 8(b) Schematic diagram of Liang regular cascode feedback resistor active inductor based VCO.

Figure 8(a) and 8(b) represents the schematics of the designed active inductor based VCOs employing feedback resistors that use the previously described cross-coupled NMOS topology for VCO. The dotted section represents the active inductor's portion, where two single ended inductors

form the differential configuration. MOS M_{neg} is used as negative resistance network which provides the high gain and it utilizes saturated MOS M_8 (acts as current source) to regulate the resistive value of M_{neg}. MOS M_{cap} is used as MOS capacitor where changing of V_{con} engenders the alternation in capacitive value of M_{cap}. $Out1$ and $Out2$ are the differential ports where outputs are taken and the supply voltage V_{DD} =1V is used to drive the network. Fig. 8(a) is VCO network that employs Weng-Kuo cascode active inductor, while Fig. 8(b) employs the Liang Feedback resistance active inductor topology. Table II represents the W/L ratios for all MOSs.

V. Simulation Results for the Proposed VCOs

TABLE II
WIDTHS AND LENGTHS OF IMPLEMENTED TRANSISTORS FOR THE PROPOSED VCOS

MOS	Width(μm)	Length(nm)
M_1	12	120
M_2	22	140
M_3	25	140
M_5	4	120
M_6	6	300
M_7	4	120
M_4	4.2	300
M_{neg}	30	100
M_8	30	100 (multipliers=3)

The designed active inductor based VCO is simulated in 90nm CMOS process with Virtuoso Cadence 6.1.6 environment. Fig. 9(a) and 9(b) show the differential output oscillation in case of control voltage $V_{con} = 0.4\,V$. Simulated results indicate that Weng-Kuo based oscillator yields a differential output of 0.468V to - 0.468 V, whereas the other one (Liang) has the value of 0.330 V to -0.330 V. This is because the power consumption of Liang Active Inductor based oscillator (1.4 mW) is less than other (2.6 mW).

The corresponding value of phase noises are -84.15 dBc/Hz (Weng-Kuo) and -80.79 dBc/Hz (Liang). Similarly, the corresponding output powers in dBm are 3.15 and 0.073 respectively.

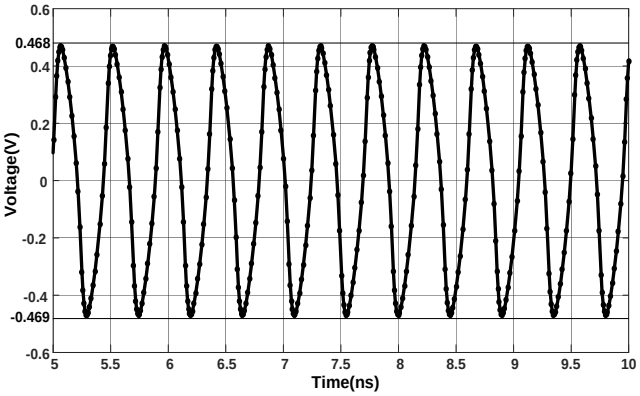

Fig. 9(a). Differential output voltage vs time for Weng-Kuo cascode active inductor based VCO.

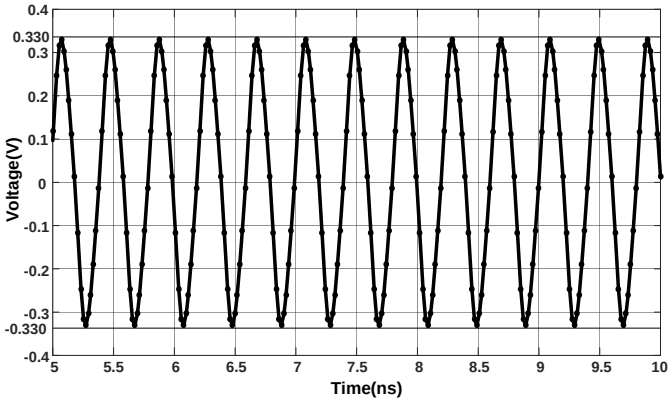

Fig. 9(b). Differential output voltage vs time for Liang regular cascode active inductor based VCO

Table III and Table IV represent the performance parameters for both of the designed active inductor based VCO for different tuning voltage ranging from 0V to 0.7 V. The first one has tuning frequency of 1.77 GHz to 2.43 GHz with a tuning scope of 31.7%. Similarly, the second one has a tuning range of 1.9 GHz to 2.52 GHz and in percentage form it is 28.28%. Both of the designs produce a frequency range that covers the operating frequency (2.4 GHz) for Bluetooth applications.

TABLE III
PERFORMANCE PARAMETERS FOR DIFFERENT TUNING VOLTAGE V_{CON}
(WENG-KUO CASCODE ACTIVE INDUCTOR BASED VCO)

V_{con} (V)	Freq. (f) GHz (PSS)	Differential Output (P-P) mV	Voltage (PSS) mV@f	Phase Noise@1Mz offset (dBc/Hz)	Power Diss.@1V (mW)	Differential Output Power (50 Ω) @f (dBm)	Figure of Merit(FoM) @1MHz Offset	
							dBc/Hz	dBF
0	1.765	482 to -482	444.9	-86.38	2.60158	2.965	-147.163	297.163
0.1	1.772	485 to -485	447.7	-86.22	2.60158	3.021	-147.037	297.037
0.2	1.817	483 to -483	454	-85.92	2.60158	3.142	-146.955	296.955
0.3	1.961	476 to -476	458.8	-85.17	2.60158	3.233	-146.867	296.867
0.4	2.216	468 to -469	454.6	-84.15	2.60158	3.153	-146.909	296.909
0.5	2.396	469 to -469	447.9	-83.84	2.60158	3.023	-147.277	297.2773
0.6	2.438	469 to -469	445.3	-83.92	2.60157	2.974	-147.508	297.508
0.7	2.430	471 to -471	444.6	-83.90	2.60157	2.959	-147.459	297.459

TABLE IV
PERFORMANCE PARAMETERS FOR DIFFERENT TUNING VOLTAGE V_{CON}
(LIANG REGULAR CASCODE ACTIVE INDUCTOR BASED VCO)

V_{con} (V)	Freq. (f) GHz (PSS)	Differ-ential Output (P-P) mV	Voltage (PSS) mV@f	Phase Noise @1Mz offset dBc/Hz	Power Diss. @1V (mW)	Differ-ential Output Power (50ohm R) @f (dBm)	Figure of Merit(FOM) @ 1MHz Offset	
							dBc/Hz	dBF
0	1.897	337 to -335	314.9	-81.95	1.39512	-0.03541	-147.163	296.065
0.1	1.940	343 to -343	316.3	-81.59	1.39512	0.00266	-145.899	295.899
0.2	2.068	339 to -339	320.7	-81.15	1.39512	0.1227	-146.015	296.014
0.3	2.310	333 to -333	322.5	-80.66	1.39512	0.1715	-146.486	296.486
0.4	2.497	330 to -330	318.9	-80.79	1.39512	0.07263	-147.292	297.292
0.5	2.543	328 to -328	317.1	-80.93	1.39512	0.02273	-147.591	297.591
0.6	2.539	330 to -330	316.5	-80.99	1.39512	0.00728	-147.637	297.637
0.7	2.522	329 to -330	316.3	-81.04	1.39512	0.863E-3	-147.629	297.629

The phase noise varies from -86.38 dBc/Hz to -83.90 dBc/Hz for the first case, where -81.95 dBC/Hz to -81.04 dBc/Hz for the second case (Fig.10). These values imply the lower sensitivity of the phase noise on the variation of tuning voltage.

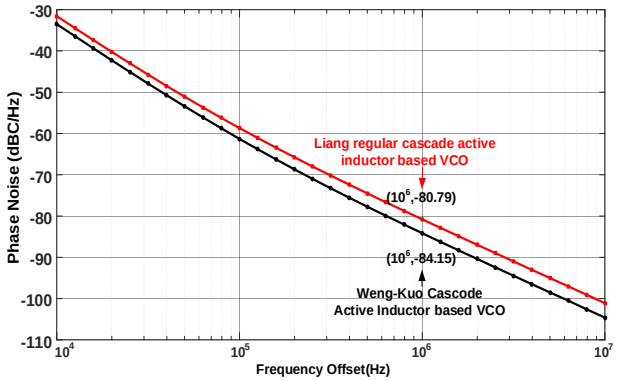

Fig. 10. Phase noise vs frequency offset for tuning voltage Vcon=0.4

A parameter that describes of performance based of the three basic performance parameters phase noise, power consumption and oscillation frequency is Figure of Merit (FoM), which is given by

$$FoM = L(\Delta\omega) + 10\log_{10}\left(\frac{P_{diss}}{1mW}\right) - 20\log_{10}\left(\frac{\omega_o}{\Delta\omega}\right)$$

Where $L\Delta(\omega)$ is the phase noise at particular offset $\Delta\omega$, ω_0 is the oscillation frequency, P_{diss} is the DC power consumption [14]. FoM can also be defined as [15]:

$$FoM(dBF) = 20\log_{10}(freq) - phase\ noise - 10\log_{10}(P_{diss})$$

Figure 11 shows the variation of frequency for different control voltages. The Weng-Kuo active inductor based oscillator has a frequency range of (1.77~ 2.43) GHz and Liang active inductor based oscillator has a frequency range of (1.9~2.52) GHz

Figure 12 shows the variation of Figure-of-Merit(FoM) with the change of tuning voltage. It is clear from the figures that the FoM is almost constant in spite of the change of tuning voltage, which indicates that the designed active inductor based oscillators have stability in performance.

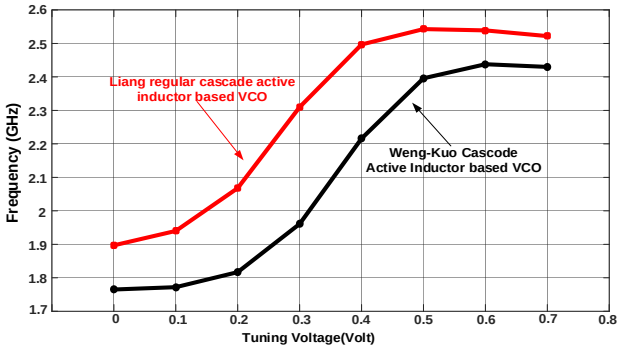

Fig. 11. Frequency vs tuning voltage for the proposed VCOs.

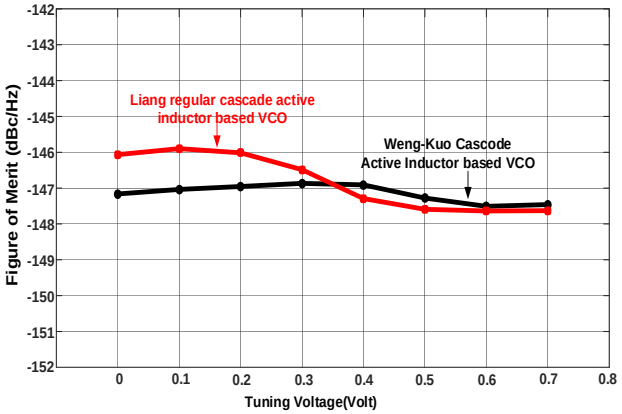

Fig. 12. Figure of merit vs tuning voltage for the proposed VCOs.

The designed VCOs use active inductor that utilizes feedback resistance topology. They consume very low power along with stability of performance which is clearly illustrated from the phase noise and FoM graph. The positive value of the output power in dBm indicates the high output power of the oscillators. Table V compares the key performance parameters of the designed VCOs with other references. Though the tuning scope is less than other references, the designed oscillator outperform the other references in terms of power consumption, output power and finally the major performance parameter FoM.

TABLE V
PERFORMANCE COMPARISON OF VCO WITH OTHER DESIGNS

References	[9]	[16]	[17]	[18]	[19]	[20]	This work (weng-Kuo)	This work (Liang)
Technology	180nm CMOS	180nm CMOS	180nm CMOS	180nm CMOS	180nm CMOS	180nm CMOS	90nm CMOS	90nm CMOS
Supply Voltage (V)	1.8	1.8	1.8	1.8	1.8	1.8	1	1
Power (mW)	44.6	16.27	29.38	11.9	28	13.8	2.60158	1.39512
Tuning Range (GHz)	1.26-2.98	0.1–2.5	-	0.55-3.8	1.325 – 2.150	0.5-2	1.765~2.430	1.897~2.52
Tuning Range(%)	81.13	184.6	-	149	47.5	120	31.7	28.28
Output Power (dBm)	-5.3 to -18.7	5 ~ 15	0.211 @ 5.5GHz	3~ -11	-16~-9	-29 to -20.8	3.153@ V_{con} =0.4V (ifferential	-0.035~ 0.000863 differential
PN@1MHz dBc/Hz)	-90	-93~ –80	-80.314	-89~-78	–86	-90 to -78	-83.38~ -86.90	-81.95 ~ -81.04
FoM (dBc/Hz) @1MHz	-141.11 @ 2.4 GHz	-120.88~ 135.84	-140.433 @ 5.5GHz	-133.5~ - 138.84	-137.5 @2GHZ	-132.6	-147.277 @2.4GHz	-147.292 @2.497 GHz

VI. CONCLUSION

Active inductor with feedback resistor based VCOs have been designed and simulated efficiently for wireless applications in 90 nm CMOS technology. Starting from the basic Graytor-C active inductor, Weng-Kuo cascode active inductor (with and without feedback resistor) and Liang regular cascode active inductor (with and without feedback resistor) topologies have been analyzed and simulated to show the inductance and quality factor. Addition of feedback resistor results in the increment of inductance as well as the quality factor whereas the values are 125.6@2.4GHz (Liang) and 98.7@3.4GHz (Weng- Kuo). The active inductor with feedback resistor techniques are then applied to design NMOS cross-coupled LC VCOs and performances are verified by simulation. Simulated results show that the Weng-Kuo active inductor based VCO has tuning frequency of 1.765GHz ~2.430GHz (31.7%), while consuming a power of 2.60 mW and phase noise of -84.15 dBc/Hz@1MHz offset, while Liang active inductor based VCO has tuning frequency of 1.897GHz ~2.522GHz (28.28%), consuming a power of 1.40 mW and phase noise of -80.79 dBc/Hz@1MHz offset.

REFERENCES

[1] D. Berny and A. M. Niknejad and R. G. Meyer, A 1.8-GHz LC VCO With 1.3-GHz Tuning Range and Digital Amplitude Calibration, IEEE JOURNAL OF SOLID-STATE CIRCUITS, vol. 40, no. 4, pp. 909-917, Aprill 2005

[2] Namrata Prasad, R. S. Gamad and C. B. Kushwah, Design of a 2.2-4.0 GHz Low Phase Noise and Low Power LC VCO, (IJCNS) International Journal of Computer and Network Security, vol. 1, no. 3, pp. 15-18, December 2009.

[3] R. M. Weng and M. Y. Sie and C. Y. Liu, A Low Power CMOS VCO for IEEE 802.11a Applications, in 2007 IEEE International Workshop on Radio-Frequency Integration Technology, Singapore, 2007, pp. 244-246.

[4] S. Diao and Y. Wang and C. Wang and F. Lin and C. H. Heng, VCO Design for Low-Power, High-Efficiency Transmitter Applications, in 2014 IEEE International Symposium on Radio-Frequency Integration Technology, Hefei, China, 2014, pp. 1-4.

[5] V. Unnikrishnan and M. Vesterbacka and A. Alvandpour, VCO-Based ADCs for IoT Applications, in 2016 International Symposium on Integrated Circuits (ISIC), Singapore, 2016, pp. 1-4.

[6] M. T. Amin, On the selection of passive elements for low phase noise LC tank VCO in 65 nm process, 2016 3rd International Conference on Electrical Engineering and Information Communication Technology (ICEEICT), Dhaka, 2016, pp. 1-5.

[7] V. Macaitis and R. Navickas, CMOS technology based LC VCO review, in 2015 Open Conference of Electrical, Electronic and Information Sciences (eStream), Vilnius, Lithuania, 2015, pp. 1-4.

[8] J. Laskar and R. Mukhopadhyay and C. H. Lee, Active Inductor-Based Oscillator: A Promising Candidate for Low-Cost Low-Power Multi-Standard Signal Generation, in 2007 IEEE Radio and Wireless Symposium, Long Beach, CA, USA, 2007, pp. 31-34

[9] J. T. Yang, S. K. Hsieh and P. J. Tsai, A Wide Tuning Range Voltage-Controlled Oscillator with Active Inductors for Bluetooth Applications, in CSS'10 Proceedings of the 4th international conference on Circuits, systems and signals, Corfu Island, Greece, 2010, pp. 39-42.

[10] R. M. Weng and R. C. Kuo, An ω0-Q Tunable CMOS Active Inductor for RF Bandpass Filters, in 2007 International Symposium on Signals, Systems and Electronics, Montreal, QC, Canada, 2007, pp. 571-574.

[11] K. Manetakis and S. M. Park and A. Payne and S. Setty and A. Thanachayanont and C. Toumazou, Wideband CMOS analog cells for video and wireless communications, in Proceedings of Third International Conference on Electronics, Circuits, and Systems, Rodos, Greece, Greece, 1996, pp. 227-230

[12] K. H. LIANG, C. C. HO, C. W. KUO and Y. J. CHAN, CMOS RF Band-Pass Filter Design Using the High Quality Active Inductor, IEICE TRANSACTIONS on Electronics, vol. E88-C, no. 12, pp. 2372-2376, Dec. 2005.

[13] M. Haase and V. Subramanian and Tao Zhang and A. Hamidian, Comparison of CMOS VCO Topologies, in 6th Conference on Ph.D. Research in Microelectronics Electronics, Berlin, Germany, 2010, pp. 1-4.

[14] J. Jalil, M. B. I. Reaz, M. A. M. Ali1 and T. G. Chang, A Low Power 3-Stage Voltage-Controlled Ring Oscillator in 0.18 µm CMOS Process for Active RFID Transponder, ELEKTRONIKA IR ELEKTROTECHNIKA, vol. 19, no. 8, pp. 69-72, 2013.

[15] T.I. Ahrens and T.H. Lee, A 1.4-GHz 3-mW CMOS LC low phase noise VCO using tapped bond wire inductances, in 1998 International Symposium on Low Power Electronics and Design, Monterey, 1998, pp. 16-19.

[16] H. B.i Kiaa, A. K. A'aina and I. Groutb, Wide tuning-range CMOS VCO based on a tunable active inductor, International Journal of Electronics, vol. 101, no. 1, pp. 88-97, December 2014.

[17] H. B.i Kiaa, A. K. A'aina and I. Groutb, Wide tuning-range CMOS VCO based on a tunable active inductor, International Journal of Electronics, vol. 101, no. 1, pp. 88-97, December 2014.

[18] N. C. Shirazi, E. Abiri and R. Hamzehyan, A 5.5 GHz Voltage Control Oscillator (VCO) with a Differential Tunable Active and Passive Inductor, International Journal of Information and Electronics Engineering, vol. 3, no. 5, pp. 493-497, September 2013.

[19] Saberkari and S. Seifollahi, Wide tuning range CMOS Colpitts VCO based on tunable active inductor, Majlesi Journal of Telecommunication Devices, vol. 1, no. 1, pp. 11-15, March 2012.

[20] G. Szczepkowski and G. Baldwin and R. Farrell, Wideband 0.18 um CMOS VCO using active inductor with negative resistance, in 2007 18th European Conference on Circuit Theory and Design, Seville, Spain, 2007, pp. 990-993.

[21] R. Mukhopadhyay and Yunseo Park and P. Sen and N. Srirattana and Jongsoo Lee and Chang-Ho Lee and S. Nuttinck and A. Joseph and J. D. Cressler and J. Laskar, Reconfigurable RFICs in Si-Based Technologies for a Compact Intelligent RF Front-End, IEEE Transactions on Microwave Theory and Techniques, vol. 53, no. 1, pp. 81-93, January 2005.